INORGANIC CHEMISTRY
FRONTIERS

RESEARCH ARTICLE

View Article Online
View Journal | View Issue

Cite this: *Inorg. Chem. Front.*, 2019, **6**, 2448

Novel osmium(II)–cymene complexes containing curcumin and bisdemethoxycurcumin ligands†

Riccardo Pettinari, *[a] Fabio Marchetti, [b] Corrado Di Nicola, [b] Claudio Pettinari, [a] Massimiliano Cuccioloni, [c] Laura Bonfili, [c] Anna Maria Eleuteri, [c] Bruno Therrien, [d] Lucinda K. Batchelor[e] and Paul J. Dyson *[e]

Received 9th July 2019,
Accepted 6th August 2019

DOI: 10.1039/c9qi00843h

rsc.li/frontiers-inorganic

The first examples of (arene)Os(II) curcuminoid derivatives have been prepared and characterized. The neutral complexes [(*p*-cym)Os(curc)Cl] (**1**) and [(*p*-cym)Os(bdcurc)Cl] (**2**), together with the cationic derivatives [(*p*-cym)Os(curc)(PTA)][SO_3CF_3] (**3**) and [(*p*-cym)Os(bdcurc)(PTA)][SO_3CF_3] (**4**) (PTA = 1,3,5-triaza-7-phosphaadamantane) were characterized by NMR spectroscopy and ESI mass spectrometry, and the crystal structure of **1** was determined by X-ray diffraction analysis. The cytotoxicity of the complexes was evaluated *in vitro* against human ovarian carcinoma cells (A2780 and A2780cisR), as well as against non-tumorous Human Embryonic Kidney cells (HEK293). Binding of the complexes to potential pharmacological targets and serum carriers was also explored.

Introduction

Cancer is one of the leading causes of death worldwide and despite severe side effects, platinum drugs are still used in the majority of chemotherapy regimens.[1,2] Other metal complexes showed promising anticancer activity and in this context half-sandwich ruthenium(II) and osmium(II) compounds are promising alternatives to platinum anticancer drugs.[3] The biological properties of half-sandwich Ru(II)- and Os(II)-complexes can be finely tuned by careful choice of the ligands directly coordinated to the metal.[4–6] Despite extensive research devoted to ruthenium complexes over the last two decades, studies on biologically active osmium complexes remain limited.[7–9] In general, osmium compounds are thought to be less cytotoxic than analogous ruthenium compounds and swapping ruthenium for the heavier congener osmium could modify the ligand exchange kinetics. Accordingly some important differences have been observed in the binding with relevant biological targets.[10] Among the families of investigated ligands, osmium-arene complexes with O,N-bidentate ligands are mostly inactive toward Human A549 lung and A2780 ovarian cancer cells[11,12] with the exception of complexes containing picolinate or 8-hydroxyquinolinate ligand.[13] Moreover, osmium-arene complexes with O,O-bidentate ligands were evaluated in anticancer assays and they possess a very low activity.[14–16] To our knowledge only a tetranuclear benzoquinonato areneosmium complex was found more active than its ruthenium analogue toward A2780 and A2780cisR cell lines.[17] On the other hand Os(II)-arene complexes with monodentate phosphine ligands were less active than the respective Ru complexes toward cancer cells.[18,19] On the contrary, complexes containing C,N-;[20] S,N-[21] or N,N-[21–25] bidentate donor ligands generally possess high antiproliferative activity. In more detail, the most potent antitumor activity is obtained when the arene-osmium fragments are bound to bioactive ligands, such as paullones,[26,27] *N*-phenylazopyridines[23] indoloquinolines[28,29] or quinoxalinones.[24] Curcumin (curcH) and bisdemethoxycurcumin (bdcurcH) are the principal active ingredients of turmeric, extracted from the plant *Curcuma longa*.[30] Curcumin has been used in traditional Oriental medicine for the treatment of different diseases due to its broad range of biological activities, including its antioxidant, anti-inflammatory and anticancer effects.[31] Although curcumin has been used in traditional Oriental medicine for the treatment of different diseases, the pharmacological application of curcumin has been quite limited because of its extremely low solubility in aqueous gastrointestinal fluids, low chemical stability at physiological pH, poor absorption in the gastrointestinal tract, and rapid metabolism in

[a]*School of Pharmacy, University of Camerino, via S. Agostino 1, 62032 Camerino MC, Italy. E-mail: riccardo.pettinari@unicam.it*
[b]*School of Science and Technology, University of Camerino, via S. Agostino 1, 62032 Camerino MC, Italy*
[c]*School of Biosciences and Veterinary Medicine, University of Camerino, Via Gentile III Da Varano, 62032 Camerino MC, Italy*
[d]*Institute of Chemistry, University of Neuchatel, Avenue de Bellevaux 51, CH-2000 Neuchatel, Switzerland*
[e]*Institut des Sciences et Ingénierie Chimiques, École Polytechnique Fédérale de Lausanne (EPFL), 1015 Lausanne, Switzerland*

†Electronic supplementary information (ESI) available. CCDC 1937799. For ESI and crystallographic data in CIF or other electronic format see DOI: 10.1039/c9qi00843h

the liver, followed by elimination through the gall bladder. In order to enhance the bioavailability and the solubility of curcumin several methods have been proposed,[32] but a very promising and innovative approach is the use of metal curcumin complexes.[33,34] We recently reported a series of half-sandwich Ru(II),[35–37] Rh(III) and Ir(III)[38] complexes bearing curcumins with promising biological activity, and the conjugation of 1,3,5-triaza-7-phosphaadamantane (RAPTA) with curcumin improved the solubility and the selectivity against tumour cell lines A2780 and A2780cisR over the non-tumorous HEK293 line.[39–41] Nevertheless, curcumin complexes have been described for all metals in the groups 7–12 except for osmium and we decided to fill this gap. Here we report the first examples of *p*-cymene-osmium(II) curcuminoid derivatives, their full solution and solid-state characterization, and an investigation of their antiproliferative potentials against human ovarian carcinoma cells relative to non-tumorous human embryonic kidney cells.

Results and discussion

Complexes **1** and **2** were prepared in high yield from the reaction of the appropriate dimer, [(*p*-cym)$OsCl_2$] with curcH/bdcurcH and KOH in methanol (Chart 1). The complexes are air-stable and soluble in alcohols, acetone, acetonitrile, chlorinated solvents, DMF and DMSO. The IR spectra of **1** and **2** show the typical shift of the ν(C=O) vibrations to lower wavenumber upon anionic ligand coordination to the metal. In the far-IR region, strong absorptions at 268 (**1**) and 245 cm^{-1} (**2**) have been assigned to ν(Os–Cl) stretches by comparison of free curcH/bdcurcH, [(*p*-cym)$OsCl_2$]$_2$ (Fig. S1–S3†) and **1** and **2** far-IR spectra (Fig. S4 and S5†). Such strong adsorptions disappear in the spectra of PTA-containing complexes **3** and **4** (Fig. S6 and S7†), similarly to analogous (arene)Ru(II) curcuminoid complexes.[37,39] The electrospray ionisation (ESI) mass spectra of **1** and **2** display peaks corresponding to the appropriate [(*p*-cym)Os(curc/bdcurc)]$^+$ ion, *i.e.* generated *via* dissociation of the chloride ligand. ^{1}H and ^{13}C chemical shifts were assigned based on the ^{1}H–^{1}H, and one-bond and long-range ^{1}H–^{13}C couplings, seen in the {^{1}H–^{1}H}-COSY, {^{1}H–^{13}C}-HSQC and {^{1}H–^{13}C}-HMBC (see ESI†). Solutions of **1** and **2** in $CDCl_3$, [D_6]DMSO and [D_6]DMSO 10%/D_2O 90% were prepared and their stability was monitored for 72 hours by NMR spectroscopy. The ^{1}H NMR spectra of **1** and **2** in $CDCl_3$ and [D_6]DMSO at 298 K show two sets of peaks due to [(*p*-cym)Os(curc/bdcurc)Cl] and the aqua complexes [(*p*-cym)Os(curc/bdcurc)(OH_2)]$^+$, similarly to arene-osmium β-diketonates previously investigate by Sadler.[15,16] The conductivity measurements confirm a partial dissociation of the chloride in DMSO at room temperature.[42] No changes were observed within 72 h (Fig. S8–S28 in ESI†). Additional studies performed at 310 K gave the same results. Further confirmation of the presence of aqua species [(*p*-cym)Os(curc/bdcurc)(OH_2)]$^+$ (**1A** and **2A** respectively) was deduced by recording the spectra of **1** and **2** in [D_6]DMSO after addition of $AgNO_3$ (and removal of AgCl by filtration) and also in [D_6]DMSO 10%/D_2O 90% (Fig. S25†).

The chloride ligand in **1** and **2** was readily replaced by the 1,3,5-triaza-7-phosphaadamantane (PTA), by treatment with a methanol solution containing equimolar $AgSO_3CF_3$ and PTA, affording [(*p*-cym)Os(curc)(PTA)][SO_3CF_3] **3** and [(*p*-cym)Os(bdcurc)(PTA)][SO_3CF_3] **4**, as depicted in Chart 2. The substitution of chloride by PTA and the formation of ionic compounds were confirmed by the disappearance of the ν(M–Cl) band in the IR spectra of **3** and **4**. Moreover, a characteristic absorption pattern in the region 1000–1200 cm^{-1}, indicative of a non-coordinated $O_3SCF_3^-$ anion, is observed.[43] The ^{1}H NMR spectra of **3** and **4** in CD_3CN and [D_6]DMSO contained only one set of resonances due to cationic [(*p*-cym)Os(curc/bdcurc)PTA]$^+$ and remain unchanged for 72 h also at 310 K. The ^{1}H NMR spectra of **3** and **4** in CD_3CN display the expected signals due to the coordinated *p*-cymene, curc/bdcurc and PTA ligands. The ^{31}P NMR resonances due to the PTA are observed at lower field with respect to those of uncoordinated PTA, thus confirming coordination to the metal center. The conductance values in CH_3CN confirm the existence of 1 : 1 electrolyte species for **3** and **4**.[42,44]

The molecular structure of complex **1** was confirmed by single-crystal X-ray structure analysis (see Experimental section and ESI† for details of the data collection and structure refinements). An ortep view of **1** is shown in Fig. 1 and the relevant geometrical parameters are reported in Table S2.† Like its ruthenium analogue,[35] the osmium atom is bound to two oxygen atoms from the chelating curc ligand, a Cl anion and the *p*-cymene, thus showing a typical piano-stool geometry.

The Ru–O distances are almost equivalent (2.092(9) Å and 2.088(9) Å), confirming an electronic delocalization of the

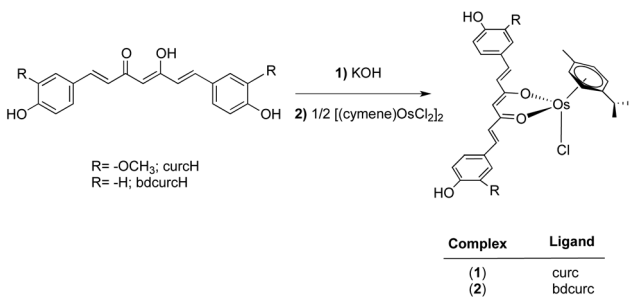

Chart 1 Synthesis of **1** and **2**.

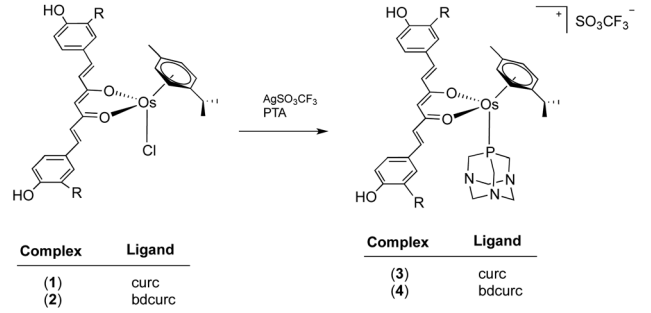

Chart 2 Synthesis of **3** and **4**.

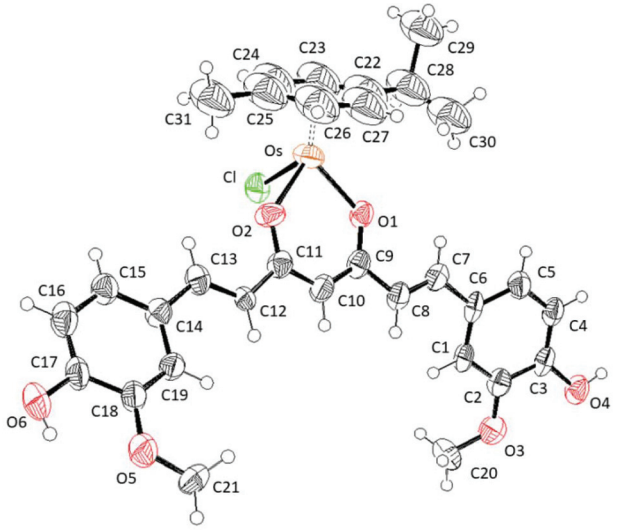

Fig. 1 Ortep view (50% probability ellipsoids) of complex **1**.

acetylacetonato group coordinated to the osmium atom. The curc ligand is not planar, the angle between the two phenyl rings being 44.8°. The *p*-cymene ligand is disordered, as emphasized by the large anisotropic displacement parameters (Fig. 1). The cytotoxicity of compounds **1–4**, curc and bdcurc was evaluated against cisplatin sensitive and cisplatin resistant human ovarian carcinoma (A2780 and A2780cisR) and non-tumoural human embryonic kidney (HEK-293) cell lines. Cisplatin and RAPTA-C were tested as positive and negative controls. IC_{50} values for the compounds, determined after 72 hours of drug exposure, are presented in Table 1.

Compound **4**, with bdcurc and PTA ligands, is the most cytotoxic of the tested compounds against the cancerous A2780 and A2780cisR cell lines. The cytotoxicity of compound **4** is comparable to that of cisplatin against the A2780 cell line, and it appears to overcome cisplatin resistance in the A2780cisR cell line with an IC_{50} value of 2.9 ± 0.2 μM compared to 29 ± 2 μM recorded for cisplatin. Compound **4** shows selectivity towards the cancer cell lines with an ~18-fold selectivity observed towards the A2780 cell line (1.9 ± 0.3 μM) compared to the HEK-293 cell line (34 ± 4 μM). In contrast, the neutral compound **2** is essentially inactive against all tested cell lines. It does, however, display modest cytotoxicity against the cisplatin resistant A2780cisR cell line with an IC_{50} of 169 ± 17 μM. Compounds **1** and **3**, containing the curc ligand, possess comparable cytotoxicity against all three cell lines, but they are less active than the free curcH proligand. However, the free curcH displays no cancer cell selectivity, whereas **1** and **3** both possess a 2-fold selectivity towards the cancerous A2780 cell line compared to the healthy HEK-293 cell line. Compound **4** is only slightly less cytotoxic than its ruthenium analogue,[39] nevertheless it retains the high selectivity towards cancerous cells that was also observed for its ruthenium analogue. In contrast, compound **2** is inactive against all tested cell lines, whereas its ruthenium analogue possesses cytotoxicity in the low micromolar range with an IC_{50} value of 0.36 ± 0.16 μM reported for the A2780 cell line.[39]

Table 1 Antiproliferative activity of **1–4**, curc, bdcurc cisplatin and RAPTA-C against cisplatin sensitive and cisplatin resistant human ovarian carcinoma (A2780 and A2780cisR) and non-tumoural human embryonic kidney (HEK-293) cell lines. IC_{50} values, recorded in μM, were measured using the MTT assay following 72 h incubation

Compound	IC_{50} (A2780) [μM]	IC_{50} (A2780cisR) [μM]	IC_{50} (HEK) [μM]
1	36 ± 3.0	39 ± 3.0	70 ± 9.0
2	>200	169 ± 17.0	>200
3	32 ± 2.0	35 ± 2.0	69 ± 7.0
4	1.9 ± 0.3	2.9 ± 0.2	34 ± 4.0
curcH	14.3 ± 1.2	18.2 ± 0.8	20 ± 1.9
bdcurcH	18.6 ± 1.2	19.4 ± 1.8	18.1 ± 1.7
cisplatin	1.5 ± 0.2	29 ± 2.0	8.8 ± 0.8
RAPTA-C	>200	>200	>200

Cell membrane permeability

Passage of **4** across the cell membrane was evaluated by monitoring the changes in membrane fluidity with a fluorescence anisotropy assay. A2780 cells treated with **4** showed an initial rapid increase in emission anisotropy, corresponding to its inclusion within cell membrane, which peaked at 20 min, slowly decreased for approximately 100 min (inclusion/internalization stationary phase) and finally rapidly returned to initial conditions after 150 min (complete cellular internalization of the molecule and recovery of initial membrane fluidity) (Fig. 2).

DNA binding

The binding of **1–4**, curcH and bdcurcH to a double-strand DNA was evaluated with a biosensor-based approach, using surface-blocked, biotin-tagged DNA as "molecular bait" for the molecules of interest. All complexes reversibly bound DNA with moderate affinity, the equilibrium dissociation constants being in the micromolar range (Table 2).

Mono-exponential binding kinetics were observed (representative superimposition of binding kinetics by increasing the concentration of **4** are shown in Fig. 3), consistent with

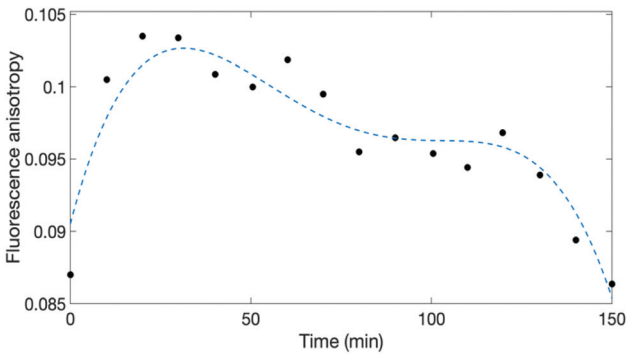

Fig. 2 Emission anisotropy variation with time upon cellular internalization of **4**.

Table 2 Kinetic and equilibrium parameters of Os complexes and parent ligands binding to surface-blocked DNA

Compound	k_{ass} (M^{-1} s^{-1})	k_{diss} (s^{-1})	K_D (μM)
1	700 ± 200	0.008 ± 0.001	11.4 ± 3.5
2	1400 ± 100	0.010 ± 0.001	7.1 ± 0.8
3	2000 ± 900	0.010 ± 0.001	5.0 ± 2.1
4	500 ± 140	0.010 ± 0.001	20.0 ± 7.8
curcH	2900 ± 650	0.014 ± 0.002	4.8 ± 1.3
bdcurcH	950 ± 300	0.010 ± 0.006	10.5 ± 7.2

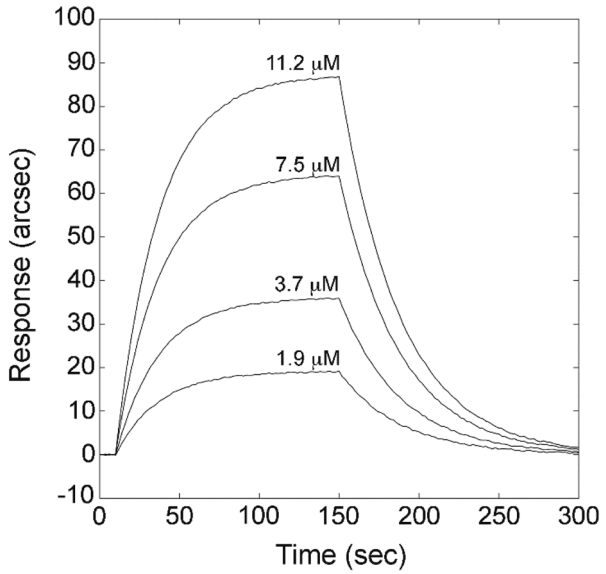

Fig. 3 Representative superimpositions of mono-exponential binding curves upon independent additions of different concentrations of **4** to DNA.

their ability to target DNA on a specific site (the biphasic model was statistically not significant at 95% confidence according to a standard *F*-test procedure). Generally, complexation of curc and bdcurc in **1–4** modestly affected their kinetics of recognition and affinity for DNA (Fig. S50†). Globally, the order of binding efficiency (expressed in terms of equilibrium dissociation constant) was: curcH = **3** > **2** > bdcurcH = **1** > **4**.

Additionally, no evident relationship exists between the observed cytotoxicity and DNA binding ability. The binding site/sites of **1–4** to DNA were investigated by performing independent competitive assays using a minor groove binder (DAPI), an intercalating agent at the minor groove (EtBr), and a major groove binder (methyl green). Globally, all compounds were able to selectively bind DNA at the minor groove, as proved by the concentration-dependent decrease in fluorescent intensity associated with the disruption of the DNA–DAPI complex (Fig. 4 and Fig. S51†). The selectivity of the binding site and the inability to intercalate between base pairs was confirmed by the lack of any significant decrease in the absorbance/fluorescence of methyl green-DNA and EtBr-DNA complexes (Fig. S52 and S53†).

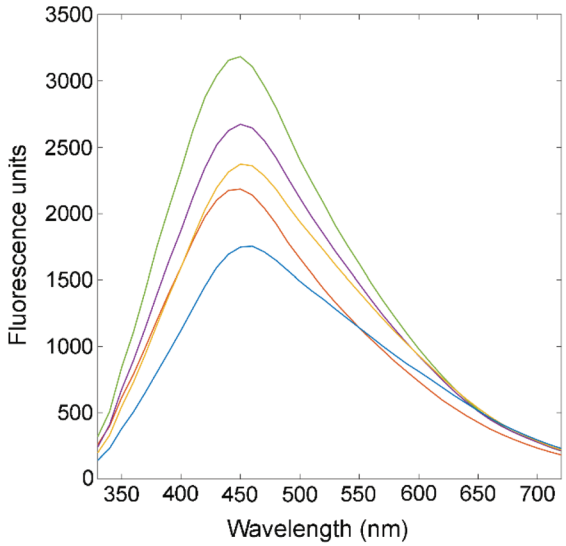

Fig. 4 Representative changes in fluorescence emission spectra of DAPI–DNA complex solution upon excitation at 338 nm (green curve) in the presence of increasing concentration of **4** the range 0–100 μM.

BSA binding

Human serum albumin (HSA) is the most abundant circulating plasma protein with an established physiological role in drug transport. In this study, bovine serum albumin (BSA) was used instead of HSA, given their high structural similarity.[45]

The binding ability of complexes **1–4** toward BSA was first evaluated according to a fluorometric assay. Upon excitation of the tryptophan residue at 295 nm, fluorescence emission spectra were recorded in the range 340–600 nm after independent addition of **1–4** and free curcH and bdcurcH. All compounds were shown to bind BSA and quench (although to different extent) its intrinsic fluorescence emission in a concentration-dependent manner (Fig. S55†). Fig. 5 shows a representative superimposition of spectra resulting from the interaction of BSA with increasing concentration of **4**. The interaction between complexes **1–4** and BSA was quantitatively characterized by using a biosensor-based assay (Table 3).

We have found that all the interactions are reversible (all complexes were dissociated upon serial washes with PBS buffer), with a general affinity for BSA in the micromolar range (Fig. S54†). Metal complexation negligibly affected kinetic and equilibrium constants for bdcurcH, parameters for **2** and **4** being quite similar. Conversely, complexes **1** and **3** showed 10-fold higher stability with respect to curcH (a representative superimposition of binding curves between BSA and **4** is reported in Fig. 6).

The order of binding efficiency (expressed in terms of equilibrium dissociation constant) was: bdcurcH = **4** > **1** = **2** = **3** > curcH.

Binding to 3-hydroxy-3-methylglutaryl-coenzyme A reductase

Tumor growth and progression are fueled by products of the mevalonate synthetic pathway, such as sterols and isopre-

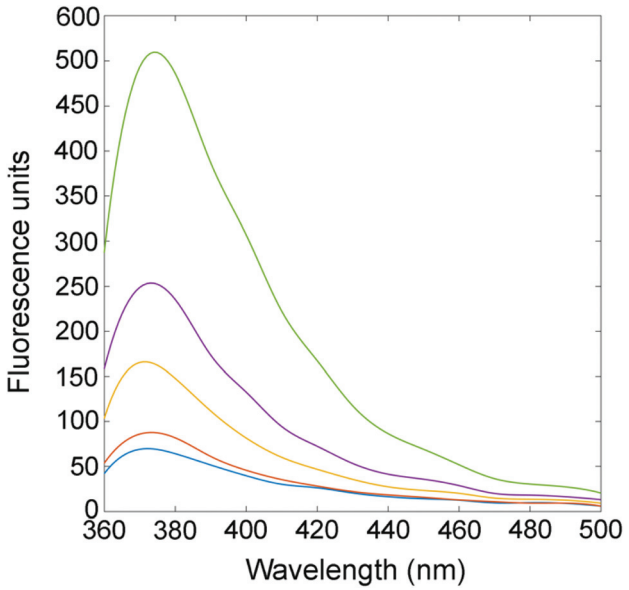

Fig. 5 Representative changes in fluorescence emission spectra of BSA (green curve) upon titration with **4** the range 0–100 μM.

Table 3 Kinetic and equilibrium parameters of Os complexes and parent ligands binding to surface-blocked BSA

Compound	k_{ass} (M^{-1} s^{-1})	k_{diss} (s^{-1})	K_D (μM)
1	2300 ± 700	0.004 ± 0.002	1.7 ± 0.7
2	2700 ± 1800	0.005 ± 0.002	1.9 ± 0.8
3	5100 ± 500	0.010 ± 0.008	2.0 ± 1.2
4	10 000 ± 800	0.005 ± 0.002	0.5 ± 0.2
curcH	3500 ± 1100	0.070 ± 0.040	20.0 ± 11.5
bdcurcH	3500 ± 1200	0.0010 ± 0.0006	0.3 ± 0.1

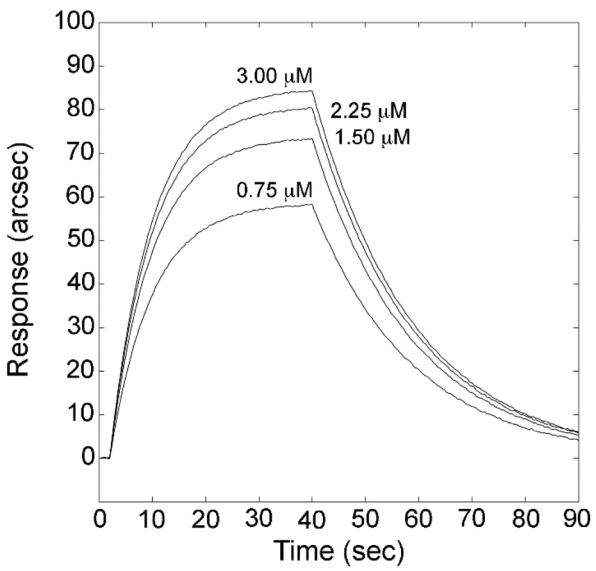

Fig. 6 Representative superimpositions of mono-exponential binding curves upon independent additions of different concentrations of **4** to BSA.

noids.[46] This pathway is rate-regulated by 3-hydroxy-3-methylglutaryl-coenzyme A reductase (HMGR), and to date, statins (potent inhibitors of HMGR, and established cholesterol-lowering drugs) have been successfully used in the treatment of some cancers.[47–49] Given the available evidences reporting HMGR inhibitory ability of metals belonging to the same group of osmium and organometallic derivatives thereof,[50,51] we evaluated the ability of the Os-complexes to bind and possibly inhibit HMGR. All complexes **1–4** bound HMGR with moderate-to-high affinity and with mono-exponential time courses, reflecting the general ability to target a specific site on the enzyme (Fig. 7 and Fig. S56†). With the only exception of **1**, the

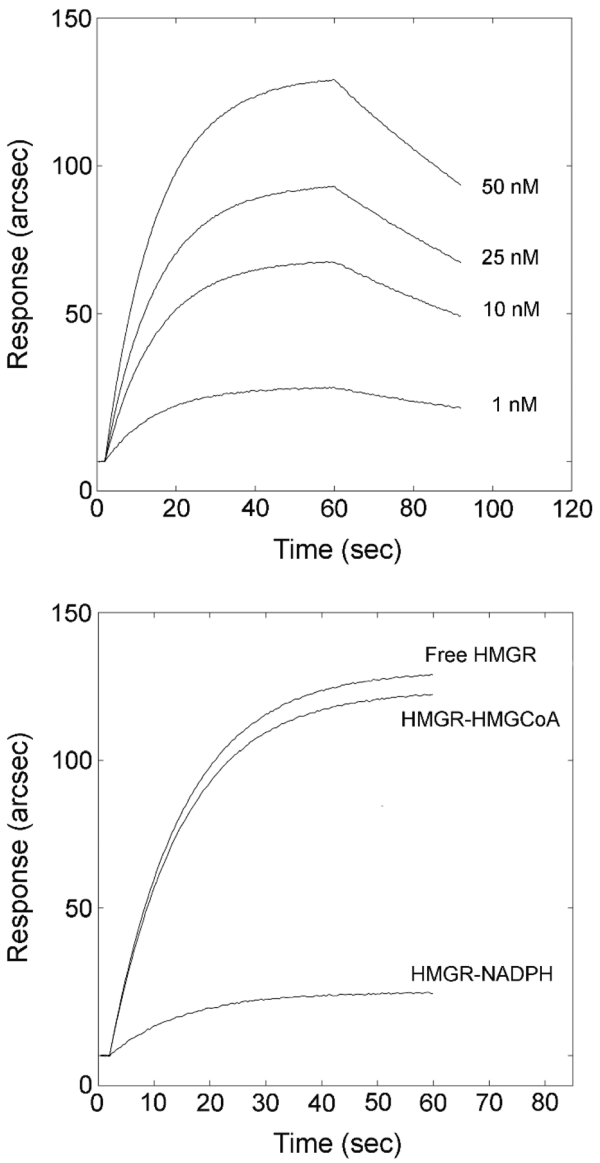

Fig. 7 Representative superimpositions of mono-exponential binding curves upon independent additions of different concentrations of **4** to HMGR (upper inset). Comparison of binding of **4** to HMGR in the presence and in the absence of saturating substrate (HMG-CoA) or cofactor (NADPH).

Table 4 Kinetic and equilibrium parameters of Os complexes and parent ligands binding to surface-blocked HMGR

Compound	k_{ass} (M^{-1} s^{-1})	k_{diss} (s^{-1})	K_D (M)
1	50 000 ± 15 000	0.025 ± 0.004	$(5.0 \pm 1.4) \times 10^{-7}$
2	110 000 ± 42 000	0.005 ± 0.001	$(4.6 \pm 1.7) \times 10^{-8}$
3	220 000 ± 90 000	0.017 ± 0.009	$(7.7 \pm 3.4) \times 10^{-8}$
4	134 000 ± 37 000	0.0010 ± 0.0006	$(7.4 \pm 3.3) \times 10^{-9}$
curcH	90 000 ± 31 000	0.04 ± 0.02	$(4.4 \pm 2.3) \times 10^{-7}$
bdcurcH	27 000 ± 10 000	0.030 ± 0.006	$(1.1 \pm 0.6) \times 10^{-6}$

complexation of curc and bdcurc strongly promoted the recognition phase and enhanced the stability of the resulting complexes **2**, **3** and **4** displaying drug-like potency (K_D in the nanomolar range – Table 4), the observed high affinity interaction being possibly responsible for the observed cytotoxicity.[52]

The order of binding efficiency (expressed in terms of equilibrium dissociation constant) was: **4** > **2** > **3** > curcH = **1** > bdcurcH. Additionally, the binding of **1–4** on HMGR were proved to occur on a region spanning the cofactor binding pocket (thus with high potential to profoundly affect enzyme activity): in fact, according to a competitive binding assay we observed that the pre-saturation of the enzyme with NADPH substantially prevented the binding of Os-curcumins to HMGR, whereas no significant effect was reported after HMG-CoA pre-saturation (Fig. 7, lower inset).

Conclusions

There has been huge public and scientific interest in the use of curcumin from the diet to reduce the risk and progression of several chronic diseases. In order to enhance the bioavailability and the solubility of curcuminoids, the use of metal curcumin complexes could be one of the most effective prospects. Here, we have reported for the first-time new *p*-cymene-osmium complexes containing curcumin-based ligands and studied their antineoplastic activity. The absence of peripheral methoxy groups in bisdemethoxycurcumin strongly influences the biological activity and, unlike analogous osmium complexes containing oxygen ligands, the cationic PTA-containing complex **4** displays high cytotoxicity in the A2780 and A2780 cisplatin-resistant tumor lines while it is not very cytotoxic on the non-tumor line. Additionally, the results of *in vitro* binding ruled out DNA as the primary target of compound **4** (all compounds showed comparably moderate affinity for the DNA probe), whereas the drug-like affinity and the binding mode displayed by compound **4** toward HMGR supported a central role of the reductase in the observed selective toxicity.

Experimental

Materials and methods

The $[(cymene)OsCl_2]_2$ was synthesized using literature methods.[53] All other materials (products) were obtained from commercial sources and were used as received. IR spectra were recorded from 4000 to 200 cm^{-1} on a PerkinElmer Frontier FT-IR instrument. ^1H, ^{13}C and ^{31}P NMR spectra were recorded with a 500 Bruker Ascend (500 MHz for ^1H, 125 MHz for ^{13}C, 202.5 MHz for ^{31}P) instrument operating at room temperature. Positive and negative ion electrospray ionization mass spectra (ESI-MS) were obtained on a Series 1100 MSI detector HP spectrometer using acetonitrile as the mobile phase. Solutions (3 mg mL^{-1}) analysis were prepared using reagent-grade acetonitrile. Masses and intensities were compared to those calculated using IsoPro Isotopic Abundance Simulator, version 2.1.28. Melting points are uncorrected and were recorded on a STMP3 Stuart scientific instrument and on a capillary apparatus. Samples for microanalysis were dried *in vacuo* to constant weight (20 °C, *ca.* 0.1 Torr) and analyzed on a Fisons Instruments 1108 CHNSO elemental analyzer.

Synthesis of the osmium complexes

[(*p*-cym)Os(curc)Cl] (1). Curcumin (93.2 mg, 0.252 mmol) was dissolved in methanol (20 mL) and KOH (14.2 mg, 0.252 mmol) was added. The mixture was stirred for 1 h at room temperature and then $[(p\text{-cym})OsCl_2]_2$ (100.0 mg, 0.126 mmol) was added. The mixture was stirred for 24 h at room temperature and an orange precipitate formed, which was removed by filtration and washed with *n*-hexane (84.8 mg, 0.116 mmol, yield 80%). The residue was concentrated to *ca.* 2 mL and stored at 4 °C. Red crystals formed over several days. Compound **1** is soluble in acetone, acetonitrile, chlorinated solvents, DMF and DMSO. Mp 188–190 °C. Anal. Calcd for $C_{31}H_{33}ClO_6Os$: C, 51.20; H, 4.57; Found: C, 51.00; H, 4.43. Λ_m (DMSO, 293 K, 10^{-4} mol L^{-1}): 13 S cm^2 mol^{-1}. IR (cm^{-1}): 3231 br ν(OH), 1619m, 1589s, 1500vs ν(C═O; C═C), 1391m, 1285s, 1233m, 1162s, 1115s, 1027s, 978vs, 865m, 585m, 474m, 455m, 268s ν(Os–Cl). ^1H NMR (CD_3Cl with 0.05% v/v TMS, 500 MHz, 298 K): δ_H, 1.37 (d, 6H, CH_3–C_6H_4–$CH(CH_3)_2$, ^3J = 6.9 Hz), 2.37 (s, 3H, CH_3–C_6H_4–$CH(CH_3)_2$), 2.83 (m, 1H, CH_3–C_6H_4–$CH(CH_3)_2$), 3.95 (s, 6H, OCH_3 curc), 5.65 (s, 1H, C(1)*H* curc), 5.81 (d, 2H, CH_3–C_6H_4–$CH(CH_3)_2$, ^3J = 5.6 Hz), 5.85 (sbr, 2H, –O*H* curc), 6.04 (d, 2H, CH_3–C_6H_4–$CH(CH_3)_2$, ^3J = 5.6 Hz), 6.42 (d, 2H, C(3, 3′)*H* curc, ^3J = 15.6 Hz), 6.92 (d, 2H, C(9, 9′)*H* curc, ^3J = 8.1 Hz), 7.03 (d, 2H, C(6, 6′)*H* curc, $^4J_{meta}$ = 1.6 Hz), 7.07 (dd, 2H, C(10, 10′)*H* curc, ^3J = 8.1 Hz, $^4J_{meta}$ = 1.6 Hz), 7.53 (d, 2H, C(4, 4′)*H* curc, ^3J = 15.6 Hz). ^{13}C NMR (CD_3Cl, 125 MHz): δ_C, 18.3 (CH_3–C_6H_4–$CH(CH_3)_2$), 22.8 (CH_3–C_6H_4–$CH(CH_3)_2$), 31.5 (CH_3–C_6H_4–$CH(CH_3)_2$), 56.0 (OCH_3 curc), 69.3 ($C_{c,c'}$ *p*-cym), 74.5 ($C_{b,b'}$ *p*-cym), 88.5 (C_d *p*-cym), 89.9 (C_a *p*-cym), 103.1 (C(1) curc), 109.1 (C(6, 6′) curc), 114.8 (C(9, 9′) curc), 122.5 (C(10, 10′) curc), 125.3 (C(3, 3′) curc), 128.5 (C(5, 5′) curc), 138.86 (C(4, 4′) curc), 146.7 (C(7, 7′) of curc), 147.3 (C(8, 8′) curc), 177.3 (C(2, 2′) curc). ESI-MS (+) CH_3CN (*m*/*z* [relative intensity, %]): 693.0 [100][(*p*-*p*-cym)Os(curc)]$^+$.

[(*p*-cym)Os(bdcurc)Cl] (2). Bisdemethoxycurcumin (77.8 mg, 0.252 mmol) was dissolved in methanol (20 mL) and KOH (14.2 mg, 0.252 mmol) was added. The mixture was stirred for 1 h at room temperature and then $[(p\text{-cym})OsCl_2]_2$ (100.0 mg, 0.126 mmol) was added. The mixture was stirred for 24 h at

room temperature and an orange precipitate formed, which was removed by filtration and washed with *n*-hexane (67.6 mg, 0.102 mmol, yield 80%). The residue was concentrated to *ca.* 2 mL and stored at 4 °C. Red crystals formed over several days. Compound **2** is soluble in acetone, acetonitrile, DMF, DMSO and is poorly soluble in chlorinated solvents. Mp 274–275 °C. Anal. Calcd for $C_{29}H_{29}ClO_4Os$: C, 52.20; H, 4.38. Found: C, 52.04; H, 4.29. Λ_m (DMSO, 293 K, 10^{-4} mol L^{-1}): 11 S cm^2 mol^{-1}. IR (cm^{-1}): 3288 br ν(OH), 1618w, 1602m, 1584m, 1500vs ν(C═O; C═C), 1396m, 1272m, 1214m, 1157s, 1103w, 990w, 826s, 553s, 514s, 481s, 253s ν(Os–Cl). ^{1}H NMR (CD_3CN with 0.05% v/v TMS, 500 MHz, 298 K): δ_H, 1.35 (d, 6H, CH_3–C_6H_4–CH(CH_3)$_2$, ^3J = 6.9 Hz), 2.29 (s, 3H, CH_3–C_6H_4–CH(CH_3)$_2$), 2.80 (m, 1H, CH_3–C_6H_4–CH(CH_3)$_2$), 5.63 (s, 1H, C(1)H bdcurc), 5.81 (d, 2H, CH_3–C_6H_4–CH(CH_3)$_2$, ^3J = 5.2 Hz), 6.08 (d, 2H, CH_3–C_6H_4–CH(CH_3)$_2$, ^3J = 5.2 Hz), 6.51 (d, 2H, C(3, 3′)H bdcurc, ^3J = 15.7 Hz), 6.87 (d, 2H, C(7, 7′)H bdcurc, ^3J = 8.4 Hz), 7.40 (sbr, 2H, –OH bdcurc), 6.51 (d, 2H, C(6, 6′)H bdcurc, ^3J = 8.4 Hz), 7.56 (d, 2H, C(4, 4′)H curc, ^3J = 15.7 Hz). ^{13}C NMR (CD_3Cl, 125 MHz): δ_C, 17.4 (CH_3–C_6H_4–CH(CH_3)$_2$), 21.9 (CH_3–C_6H_4–CH(CH_3)$_2$), 29.9 (CH_3–C_6H_4–CH(CH_3)$_2$), 69.5 ($C_{c,c'}$ *p*-cym), 74.3 ($C_{b,b'}$ *p*-cym), 89.5 (C_d *p*-cym), 94.0 (C_a *p*-cym), 103.3 (C(1) bdcurc), 115.8 (C(7, 7′) bdcurc), 124.5 (C(3, 3′) bdcurc), 127.7 (C(5, 5′) bdcurc), 129.9 (C(6, 6′) bdcurc), 138.3 (C(4, 4′) bdcurc), 158.6 (C(8, 8′) bdcurc), 177.1 (C(2, 2′) bdcurc). ESI-MS (+) CH_3CN (*m*/*z* [relative intensity, %]): 633.0 [100][(*p*-cym)Os(bdcurc)]$^+$.

[(*p*-cym)Os(curc)(PTA)]SO_3CF_3 (3). Compound **1** (54.5 mg, 0.075 mmol) was dissolved in methanol (10 mL) and $AgCF_3SO_3$ (19.1 mg, 0.075 mmol) was added. The mixture was stirred for 2 h at 298 K and filtered to remove AgCl. PTA (PTA = 1,3,5-triaza-7-phosphaadamantane; 11.75 mg, 0.075 mmol) was then added to the filtrate and the resulting mixture was stirred for 24 h at room temperature. Then the solution was dried by rotary evaporation and dichloromethane (2 mL) and an excess of *n*-hexane were added. The mixture was left at 4 °C until a yellow precipitate formed. The powder was recovered by filtration and air-dried. Compound **3** (54.6 mg, 0.054 mmol, yield 72%), is soluble in alcohols, acetone, acetonitrile, chlorinated solvents, DMF and DMSO and slightly soluble in water. Mp 185–187 °C. Anal. Calcd for $C_{38}H_{45}F_3N_3O_9OsPS$: C, 45.73; H, 4.54; F, 5.71. Found: 45.55; H, 4.50; F, 5.56. Λ_m (DMSO, 293 K, 10^{-4} mol L^{-1}): 45 S cm^2 mol^{-1}. ^{1}H NMR (CD_3CN with 0.05% v/v TMS, 500 MHz, 298 K): δ_H, 1.37 (d, 6H, CH_3–C_6H_4–CH(CH_3)$_2$, ^3J = 6.9 Hz), 2.20 (s, 3H, CH_3–C_6H_4–CH(CH_3)$_2$), 2.71 (m, 1H, CH_3–CH_4–CH(CH_3)$_2$), 3.95 (s, 6H, OCH_3 curc), 4.11 (sbr, 6H, NCH_2P, PTA), 4.5 (dd, 6H, NCH_2N, PTA), 5.85 (s, 1H, C(1)H curc), 5.90 (d, 2H, CH_3–C_6H_4–CH(CH_3)$_2$, ^3J = 5.7 Hz), 5.99 (d, 2H, CH_3–C_6H_4–CH(CH_3)$_2$, ^3J = 5.7 Hz), 6.62 (d, 2H, C(3, 3′)H curc, ^3J = 15.6 Hz), 6.89 (d, 2H, C(9, 9′)H curc, ^3J = 8.1 Hz), 7.15 (dd, 2H, C(10, 10′)H curc, ^3J = 8.1 Hz, $^4J_{meta}$ = 1.5 Hz), 7.28 (d, 2H, C(6, 6′)H curc, $^4J_{meta}$ = 1.5 Hz), 7.50 (d, 2H, C(4, 4′) H curc, ^3J = 15.6 Hz). ^{13}C NMR (CD_3CN, 125 MHz): δ_C, 17.3 (CH_3–C_6H_4–CH(CH_3)$_2$), 22.7 (CH_3–C_6H_4–CH(CH_3)$_2$), 31.4 (CH_3–C_6H_4–CH(CH_3)$_2$), 51.2 (d, P–CH_2–N, PTA, J = 18.9 Hz), 56.9 (OCH_3 curc), 73.2 (d, N–CH_2–N, PTA, J = 7.3 Hz),81.9 ($C_{c,c'}$ *p*-cym), 82.8 ($C_{b,b'}$ *p*-cym), 89.8 (C_a *p*-cym), 95.7 (C_d *p*-cym), 106.7 (C(1) curc), 111.2 (C(6, 6′) curc), 116.2 (C(9, 9′) curc), 124.2 (C(10, 10′) curc), 124.3 (C(3, 3′) curc), 128.9 (C(5, 5′) curc), 141.4 (C(4, 4′) curc), 148.9 (C(7, 7′) of curc), 149.7 (C(8, 8′) curc), 179.7 (C(2, 2′) curc). ^{31}P NMR (CD_3CN, 293 K): δ −66.7. ESI-MS (+) CH_3CN (*m*/*z* [relative intensity, %]): 850.0 [100] [(*p*-cym)Os(curc)(PTA)]$^+$.

[(*p*-cym)Os(bdcurc)(PTA)]SO_3CF_3 (4). Compound **2** (50.0 mg, 0.075 mmol) was dissolved in methanol (10 mL) and $AgCF_3SO_3$ (19.1 mg, 0.075 mmol) was added. The mixture was stirred for 2 h at 298 K and filtered to remove AgCl. PTA (PTA = 1,3,5-triaza-7-phosphaadamantane; 11.75 mg, 0.075 mmol) was then added to the filtrate and the resulting mixture was stirred for 24 h at room temperature. Then the solution was dried by rotary evaporation and dichloromethane (2 mL) and an excess of *n*-hexane were added. The mixture was left at 4 °C until a yellow precipitate formed. The powder was recovered by filtration and air-dried. Compound **4** (50.05 mg, 0.053 mmol, yield 70%) is soluble in alcohols, acetone, acetonitrile, chlorinated solvents, DMF and DMSO and slightly soluble in water. 197–198. Anal. Calcd for $C_{36}H_{41}F_3N_3O_7OsPS$: C, 46.10; H, 4.41; F, 6.08. Found: C, 46.02; H, 4.37; F, 6.01. Λ_m (DMSO, 293 K, 10^{-4} mol L^{-1}): 48 S cm^2 mol^{-1}. IR (cm^{-1}): 3200 br ν(OH), 1604m, 1498 vs ν(C═O; C═C), 1395w, 1240m, 1027m, 996w, 828m, 575s, 552m, 516s, 483s, 458m. ^{1}H NMR (CD_3CN, 293 K): δ, 1.36 (d, 6H, CH_3–C_6H_4–CH(CH_3)$_2$, ^3J = 6.9 Hz), 2.19 (s, 3H, CH_3–C_6H_4–CH(CH_3)$_2$), 2.70 (m, 1H, CH_3–C_6H_4–CH(CH_3)$_2$), 4.10 (s, 6H, NCH_2P, PTA), 4.42 and 4.52 (dd, 6H, NCH_2N, PTA), 5.84 (s, 1H, C(1)H bdcurc), 5.90 (d, 2H, CH_3–C_6H_4–CH(CH_3)$_2$, ^3J = 5.7 Hz), 5.99 (d, 2H, CH_3–C_6H_4–CH(CH_3)$_2$, ^3J = 5.7 Hz), 6.57 (d, 2H, C(3, 3′)H bdcurc, ^3J = 15.6 Hz), 6.89 (d, 4H, C(7, 7′)H bdcurc, ^3J = 8.6 Hz), 7.40 (br, 2H, –OH bdcurc), 7.51 (d, 2H, C(4, 4′)H bdcurc, ^3J = 15.6 Hz), 7.55 (d, 4H, C(6, 6′)H bdcurc, ^3J = 8.6 Hz). ^{13}C NMR (CD_3CN, 293 K): δ 16.2 (CH_3–C_6H_4–CH(CH_3)$_2$), 21.7 (CH_3–C_6H_4–CH(CH_3)$_2$), 30.3 (CH_3–C_6H_4–CH(CH_3)$_2$), 50.1 (d, P-CH_2-N, PTA, J = 19.0 Hz), 72.1 (d, N-CH_2-N, PTA, J = 7.2 Hz), 80.8 ($C_{c,c'}$ *p*-cym), 81.7 ($C_{b,b'}$ *p*-cym), 88.6 (C_d *p*-cym), 94.5 (C_a *p*-cym), 105.6 (C(1) bdcurc), 116.0 (C(7, 7′) bdcurc), 122.9 (C(3, 3′) bdcurc), 127.5 (C(5, 5′) bdcurc), 130.0 (C(6, 6′) bdcurc), 140.0 (C(4, 4′) bdcurc), 159.1 (C(8, 8′) bdcurc), 178.7 (C(2, 2′) bdcurc). ^{31}P NMR (CD_3CN, 293 K): δ −65.9. ESI-MS (+) CH_3CN (*m*/*z* [relative intensity, %]): 790.0 [100][(*p*-cym)Os(bdcurc)(PTA)]$^+$.

Single-crystal X-ray structure analysis

A crystal of compound **1** was mounted on a Stoe Image Plate Diffraction system equipped with a ϕ circle goniometer, using Mo-Kα graphite monochromated radiation (λ = 0.71073 Å) with ϕ range 0–200°. The structure was solved by direct methods using the program SHELXS, while refinement and all further calculations were carried out using SHELXL.[54] The H-atoms were included in calculated positions and treated as riding atoms using the SHELXL default parameters. The non-H atoms were refined anisotropically, using weighted full-matrix least-square on F^2. In complex **1**, the *p*-cymene ligand was disordered and equal anisotropic displacement para-

meters were used to avoid highly elongated ellipsoids. The remaining large residual electronic densities are located near the osmium atom. Crystallographic details are summarized in Table S1.† Fig. 1 was drawn with ORTEP-32.[55] CCDC 1937799† contains the supplementary crystallographic data for this paper.

Cell culture and cytotoxicity studies

Human ovarian carcinoma (A2780 and A2780cisR) cell lines were obtained from the European Collection of Cell Cultures. The human embryonic kidney (HEK-293) cell line was obtained from ATCC (Sigma, Buchs, Switzerland). Penicillin streptomycin, RPMI 1640 GlutaMAX (where RPMI = Roswell Park Memorial Institute), and DMEM GlutaMAX media (where DMEM = Dulbecco's modified Eagle medium) were obtained from Life Technologies, and fetal bovine serum (FBS) was obtained from Sigma. The cells were cultured in RPMI 1640 GlutaMAX (A2780 and A2780cisR) and DMEM GlutaMAX (HEK-293) media containing 10% heat-inactivated FBS and 1% penicillin streptomycin at 37 °C and CO_2 (5%). The A2780cisR cell line was routinely treated with cisplatin (2 μM) in the media to maintain cisplatin resistance. The cytotoxicity was determined using the 3-(4,5-dimethyl-2-thiazolyl)-2,5-diphenyl-2*H*-tetrazolium bromide (MTT) assay.[56] Cells were seeded in flat-bottomed 96-well plates as a suspension in a prepared medium (100 μL aliquots and approximately 4300 cells per well) and preincubated for 24 h. Stock solutions of compounds were prepared in DMSO and were diluted in medium. The solutions were sequentially diluted to give a final DMSO concentration of 0.5% and a final compound concentration range (0–200 μM). Cisplatin and RAPTA-C were tested as a positive (0–100 μM) and negative (200 μM) controls respectively. The compounds were added to the preincubated 96-well plates in 100 μL aliquots, and the plates were incubated for a further 72 h. MTT (20 μL, 5 mg mL^{-1} in Dulbecco's phosphate buffered saline) was added to the cells, and the plates were incubated for a further 4 h. The culture medium was aspirated and the purple formazan crystals, formed by the mitochondrial dehydrogenase activity of vital cells, were dissolved in DMSO (100 μL per well). The absorbance of the resulting solutions, directly proportional to the number of surviving cells, was quantified at 590 nm using a SpectroMax M5e multimode microplate reader (using SoftMax Pro software, version 6.2.2). The percentage of surviving cells was calculated from the absorbance of wells corresponding to the untreated control cells. The reported IC_{50} values are based on the means from two independent experiments, each comprising four tests per concentration level.

Fluorescence anisotropy measurements

The change in membrane fluidity of A2780 cells treated with 10 μM complex 4 was monitored using TMA-DPH fluorescent probe (λ_{exc} = 340 nm; λ_{em} = 460 nm).[57] Anisotropy measurements were carried out at 37 °C on a RF-5301PC Shimadzu spectrofluorimeter. In detail, 1.5×10^5 A2780 cells per mL were incubated with 4, and 1 μM TMA-DPH was added at 37 °C. Fluorescence anisotropy (r) was measured for 200 min, and was calculated from the following equation:

$$r = \frac{2P}{3 - P}$$

Fluorescence polarization (P) was derived using the equation:

$$P = \frac{I_{\parallel} - I_{\perp}}{I_{\parallel} + I_{\perp}}$$

with $I_{\parallel}$ and $I_{\perp}$ being the fluorescence intensities parallel and perpendicular to the excitation beam, respectively.

BSA quenching

Quenching of BSA tryptophan fluorescence was used to study the interaction between serum albumin and the compounds of interest. Fluorescence spectra of 10 μM BSA were recorded from 300 nm to 450 nm upon tryptophan excitation at 295 nm.[58] Fluorometric titrations were performed by individual additions of Os complexes and parent compounds thereof in the range 1–10 μM. All titrations were performed at 37 °C.

DNA binding

The DNA binding ability of Os complexes along with parent curcumins was tested on an IAsys plus biosensor. DNA sensing surfaces (DNA sequence: 3′-CCACCCACTACCCTGGTTGGA-TG-CTAATGT-5′) were obtained as previously described.[59] The compounds of interest were independently added to DNA coated surface at different concentrations, each time following binding kinetics up to equilibrium. Dissociation steps were performed by a single 1 min wash with fresh PBS buffer, whereas free DNA surface regeneration was achieved by serial PBS washes, each time assessing the recovery of free DNA baseline prior to any further addition of the compounds of interest. The biosensor chamber was thermostatted at 37 °C throughout. Raw data were globally fitted to both mono- and bi-exponential models, and the validity of each model to fit time courses was assessed by a standard F-test procedure.

DNA competitive binding assays

Three independent displacement assays were used to dissect the binding geometry of Os-DNA complexes. DNA molecules were individually labelled with 4,6-diamidino-2-phenylindole (DAPI, a minor groove binder), [4-([4-(dimethylamino)phenyl]{4-[ethyl(dimethyl)ammonio]phenyl}methylene)-2,5 cyclohexadien-1-ylidene](dimethyl)ammonium chloride (methyl green, a major groove binder), and 3,8-diamino-5-ethyl-6-phenylphenanthridinium bromide (ethidium bromide, an intercalating agent) as previously reported[59] and resulting DNA complexes were challenged with increasing concentration of Os complexes and parent curcumins. Briefly, DAPI displacement was monitored by recording the emission spectra of solutions containing different concentrations of the molecules of interest (0–100 μM), DNA (20 μM), and DAPI (15 μM) in phosphate buffer (10 mM, pH 7.4). Methyl green displacement assay was performed by monitoring the absorbance at 630 nm upon

addition of the candidate competitors. EtBr displacement was performed by recording the changes in the emission spectra of solutions containing different concentrations of the molecules of interest (0–100 μM), DNA (20 μM), and EtBr (10 μM) in phosphate buffer (pH 7.4). All experiments were run at room temperature.

HMGR binding

Biosensor surface containing HMGR was prepared as previously described.[60] Surface-blocked HMGR was tested for binding to the compounds of interest at different concentrations in the range 1–50 nM, essentially according to the same procedure described for the DNA-based biosensor. The preservation of the native-like conformation/functionality of the enzyme upon immobilization and the identification of the site of binding for Os complexes was assessed using HMGR physiological substrates, namely HMG-CoA and NADPH. The biosensor chamber was thermostatted at 37 °C throughout. Raw data were analyzed with mono- and bi-exponential models, the validity of each model to fit time courses being assessed by *F*-test procedure.

Statistical analysis

Results presented in this study are expressed as mean values with their standard deviations obtained from tree separate experiments. Statistical analysis was performed with one-way ANOVA, followed by the Bonferroni test using Sigma-stat 3.1 software (SPSS, Chicago, IL). p-Values < 0.05 were considered significant.

Conflicts of interest

There are no conflicts to declare.

Acknowledgements

This work was financially supported by the University of Camerino (Fondo di Ateneo per la Ricerca 2018).

References

1 R. L. Siegel, K. D. Miller and A. Jemal, *Cancer J. Clin.*, 2016, **66**, 7–30.
2 N. J. Wheate, S. Walker, G. E. Craig and R. Oun, *Dalton Trans.*, 2010, **39**, 8113–8127.
3 E. Alessio, *Bioinorganic Medicinal Chemistry*, John Wiley & Sons, Ltd, 2011.
4 S. M. Meier-Menches, C. Gerner, W. Berger, C. G. Hartinger and B. K. Keppler, *Chem. Soc. Rev.*, 2018, **47**, 909–928.
5 L. Zeng, P. Gupta, Y. Chen, E. Wang, L. Ji, H. Chao and Z.-S. Chen, *Chem. Soc. Rev.*, 2017, **46**, 5771–5804.
6 S. K. Singh and D. S. Pandey, *RSC Adv.*, 2014, **4**, 1819–1840.
7 P. Zhang and H. Huang, *Dalton Trans.*, 2018, **47**, 14841–14854.
8 R. Pettinari, F. Marchetti, C. Di Nicola and C. Pettinari, *Eur. J. Inorg. Chem.*, 2018, 3521–3536.
9 M. Hanif, M. V. Babak and C. G. Hartinger, *Drug Discovery Today*, 2014, **19**, 1640–1648.
10 A. Casini, F. Edafe, M. Erlandsson, L. Gonsalvi, A. Ciancetta, N. Re, A. Ienco, L. Messori, M. Peruzzini and P. J. Dyson, *Dalton Trans.*, 2010, **39**, 5556–5563.
11 S. H. van Rijt, A. J. Hebden, T. Amaresekera, R. J. Deeth, G. J. Clarkson, S. Parsons, P. C. McGowan and P. J. Sadler, *J. Med. Chem.*, 2009, **52**, 7753–7764.
12 S. H. van Rijt, A. F. A. Peacock, R. D. L. Johnstone, S. Parsons and P. J. Sadler, *Inorg. Chem.*, 2009, **48**, 1753–1762.
13 A. F. A. Peacock, S. Parsons and P. J. Sadler, *J. Am. Chem. Soc.*, 2007, **129**, 3348–3357.
14 M. Hanif, H. Henke, S. M. Meier, S. Martic, M. Labib, W. Kandioller, M. A. Jakupec, V. B. Arion, H.-B. Kraatz, B. K. Keppler and C. G. Hartinger, *Inorg. Chem.*, 2010, **49**, 7953–7963.
15 A. F. A. Peacock, M. Melchart, R. J. Deeth, A. Habtemariam, S. Parsons and P. J. Sadler, *Chem. - Eur. J.*, 2007, **13**, 2601–2613.
16 A. F. A. Peacock, A. Habtemariam, R. Fernández, V. Walland, F. P. A. Fabbiani, S. Parsons, R. E. Aird, D. I. Jodrell and P. J. Sadler, *J. Am. Chem. Soc.*, 2006, **128**, 1739–1748.
17 N. P. E. Barry, F. Edafe, P. J. Dyson and B. Therrien, *Dalton Trans.*, 2010, **39**, 2816–2820.
18 A. Dorcier, W. H. Ang, S. Bolaño, L. Gonsalvi, L. Juillerat-Jeannerat, G. Laurenczy, M. Peruzzini, A. D. Phillips, F. Zanobini and P. J. Dyson, *Organometallics*, 2006, **25**, 4090–4096.
19 M. Hanif, A. A. Nazarov, C. G. Hartinger, W. Kandioller, M. A. Jakupec, V. B. Arion, P. J. Dyson and B. K. Keppler, *Dalton Trans.*, 2010, **39**, 7345–7352.
20 C. A. Riedl, L. S. Flocke, M. Hejl, A. Roller, M. H. M. Klose, M. A. Jakupec, W. Kandioller and B. K. Keppler, *Inorg. Chem.*, 2017, **56**, 528–541.
21 S. M. Meier, M. Hanif, Z. Adhireksan, V. Pichler, M. Novak, E. Jirkovsky, M. A. Jakupec, V. B. Arion, C. A. Davey, B. K. Keppler and C. G. Hartinger, *Chem. Sci.*, 2013, **4**, 1837–1846.
22 L. K. Filak, S. Göschl, P. Heffeter, K. Ghannadzadeh Samper, A. E. Egger, M. A. Jakupec, B. K. Keppler, W. Berger and V. B. Arion, *Organometallics*, 2013, **32**, 903–914.
23 Y. Fu, A. Habtemariam, A. M. B. H. Basri, D. Braddick, G. J. Clarkson and P. J. Sadler, *Dalton Trans.*, 2011, **40**, 10553–10562.
24 W. Ginzinger, G. Mühlgassner, V. B. Arion, M. A. Jakupec, A. Roller, M. Galanski, M. Reithofer, W. Berger and B. K. Keppler, *J. Med. Chem.*, 2012, **55**, 3398–3413.
25 Y. Fu, A. Habtemariam, A. M. Pizarro, S. H. van Rijt, D. J. Healey, P. A. Cooper, S. D. Shnyder, G. J. Clarkson and P. J. Sadler, *J. Med. Chem.*, 2010, **53**, 8192–8196.

26 W. F. Schmid, R. O. John, G. Mühlgassner, P. Heffeter, M. A. Jakupec, M. Galanski, W. Berger, V. B. Arion and B. K. Keppler, *J. Med. Chem.*, 2007, **50**, 6343–6355.
27 W. F. Schmid, R. O. John, V. B. Arion, M. A. Jakupec and B. K. Keppler, *Organometallics*, 2007, **26**, 6643–6652.
28 L. K. Filak, G. Mühlgassner, M. A. Jakupec, P. Heffeter, W. Berger, V. B. Arion and B. K. Keppler, *JBIC, J. Biol. Inorg. Chem.*, 2010, **15**, 903–918.
29 L. K. Filak, G. Mühlgassner, F. Bacher, A. Roller, M. Galanski, M. A. Jakupec, B. K. Keppler and V. B. Arion, *Organometallics*, 2011, **30**, 273–283.
30 T. Esatbeyoglu, P. Huebbe, I. M. A. Ernst, D. Chin, A. E. Wagner and G. Rimbach, *Angew. Chem., Int. Ed.*, 2012, **51**, 5308–5332.
31 M. Salem, S. Rohani and E. R. Gillies, *RSC Adv.*, 2014, **4**, 10815–10829.
32 S. Prasad, A. K. Tyagi and B. B. Aggarwal, *Cancer Res. Treat.*, 2014, **46**, 2–18.
33 S. Banerjee and A. R. Chakravarty, *Acc. Chem. Res.*, 2015, **48**, 2075–2083.
34 S. Wanninger, V. Lorenz, A. Subhan and F. T. Edelmann, *Chem. Soc. Rev.*, 2015, **44**, 4986–5002.
35 F. Caruso, M. Rossi, A. Benson, C. Opazo, D. Freedman, E. Monti, M. B. Gariboldi, J. Shaulky, F. Marchetti, R. Pettinari and C. Pettinari, *J. Med. Chem.*, 2012, **55**, 1072–1081.
36 R. Pettinari, F. Marchetti, C. Pettinari, P. Smoleński, T. Riedel, R. Scopelliti and P. J. Dyson, *Eur. J. Inorg. Chem.*, 2017, 2905–2910.
37 R. Pettinari, A. Petrini, F. Marchetti and D. Nicola, *ChemistrySelect*, 2018, **3**, 6696–6700.
38 R. Pettinari, F. Marchetti, C. Pettinari, F. Condello, A. Petrini, R. Scopelliti, T. Riedel and P. J. Dyson, *Dalton Trans.*, 2015, **44**, 20523–20531.
39 R. Pettinari, F. Marchetti, F. Condello, C. Pettinari, G. Lupidi, R. Scopelliti, S. Mukhopadhyay, T. Riedel and P. J. Dyson, *Organometallics*, 2014, **33**, 3709–3715.
40 S. Huang, H. Li, Y. Liu, Y. Liang, W. Su and Q. Xiao, *Polyhedron*, 2019, **167**, 51–61.
41 S. Huang, J. Xie, W. Su, Y. Liu, X. Wang, B. Hu and Q. Xiao, *J. Organomet. Chem.*, 2017, **853**, 81–92.
42 J. Palmucci, F. Marchetti, R. Pettinari, C. Pettinari, R. Scopelliti, T. Riedel, B. Therrien, A. Galindo and P. J. Dyson, *Inorg. Chem.*, 2016, **55**, 11770–11781.
43 K. Nakamoto, *Infrared and Raman spectra of inorganic and coordination compounds*, Wiley, New York (N.Y.), 5th edn, 1997, pp. 1922–2011.
44 W. J. Geary, *Coord. Chem. Rev.*, 1971, **7**, 81–122.
45 J. R. Brown, *Fed. Proc.*, 1976, **35**, 2141–2144.
46 G. Llaverias, C. Danilo, I. Mercier, K. Daumer, F. Capozza, T. M. Williams, F. Sotgia, M. P. Lisanti and P. G. Frank, *Am. J. Pathol.*, 2011, **178**, 402–412.
47 A. Hoque, H. Chen and X. Xu, *Cancer Epidemiol., Biomarkers Prev.*, 2008, **17**, 88–94.
48 A. Parikh, C. Childress, K. Deitrick, Q. Lin, D. Rukstalis and W. Yang, *Prostate*, 2010, **70**, 971–981.
49 H.-Y. Chen, Q. Wang, Q.-H. Xu, L. Yan, X.-F. Gao, Y.-H. Lu and L. Wang, *BioMed Res. Int.*, 2016, **2016**, 9125238.
50 T. Kawachi and H. Rudney, *Biochemistry*, 1970, **9**, 1700–1705.
51 M. Cuccioloni, L. Bonfili, M. Mozzicafreddo, V. Cecarini, R. Pettinari, F. Condello, C. Pettinari, F. Marchetti, M. Angeletti and A. M. Eleuteri, *RSC Adv.*, 2016, **6**, 39636–39641.
52 T. Carbonell and E. Freire, *Biochemistry*, 2005, **44**, 11741–11748.
53 H. Werner and K. Zenkert, *J. Organomet. Chem.*, 1988, **345**, 151–166.
54 G. M. Sheldrick, *Acta Crystallogr., Sect. C: Struct. Chem.*, 2015, **71**, 3–8.
55 L. J. Farrugia, *J. Appl. Crystallogr.*, 1997, **30**, 565.
56 T. Mosmann, *J. Immunol. Methods*, 1983, **65**, 55–63.
57 J.-G. Kuhry, P. Fonteneau, G. Duportail, C. Maechling and G. Laustriat, *Cell Biophys.*, 1983, **5**, 129–140.
58 D. E. Epps, T. J. Raub, V. Caiolfa, A. Chiari and M. Zamai, *J. Pharm. Pharmacol.*, 1999, **51**, 41–48.
59 R. Pettinari, C. Pettinari, F. Marchetti, B. W. Skelton, A. H. White, L. Bonfili, M. Cuccioloni, M. Mozzicafreddo, V. Cecarini, M. Angeletti, M. Nabissi and A. M. Eleuteri, *J. Med. Chem.*, 2014, **57**, 4532–4542.
60 M. Cuccioloni, M. Mozzicafreddo, M. Spina, C. N. Tran, M. Falconi, A. M. Eleuteri and M. Angeletti, *J. Lipid Res.*, 2011, **52**, 897–907.